nature chemistry

ARTICLES

PUBLISHED ONLINE: 24 OCTOBER 2010 | DOI: 10.1038/NCHEM.871

Storable, thermally activated, near-infrared chemiluminescent dyes and dye-stained microparticles for optical imaging

Jeffrey M. Baumes, Jeremiah J. Gassensmith, Jay Giblin, Jung-Jae Lee, Alexander G. White, William J. Culligan, W. Matthew Leevy, Masaru Kuno and Bradley D. Smith*

Imaging techniques are a vital part of clinical diagnostics, biomedical research and nanotechnology. Optical molecular imaging makes use of relatively harmless, low-energy light and technically straightforward instrumentation. Self-illuminating, chemiluminescent systems are particularly attractive because they have inherently high signal contrast due to the lack of background emission. Currently, chemiluminescence imaging involves short-lived molecular species that are not stored but are instead generated *in situ*, and they typically emit visible light, which does not penetrate far through heterogeneous biological media. Here, we describe a new paradigm for optical molecular imaging using squaraine rotaxane endoperoxides, interlocked fluorescent and chemiluminescent dye molecules that have a squaraine chromophore encapsulated inside a macrocycle endoperoxide. Squaraine rotaxane endoperoxides can be stored indefinitely at temperatures below −20 °C, but upon warming to body temperature they undergo a unimolecular chemical reaction and emit near-infrared light that can pass through a living mouse.

Radiotracers are molecular probes containing radioactive isotopes, the high-energy emission of which can be detected at extremely low concentrations[1]. The radioisotopes are typically generated and detected using sophisticated equipment, and some radioisotopes, particularly positron emitters, decay rapidly, thus limiting their shelf-life. High-energy radiation readily passes through skin and tissue, a feature that is valuable for medical imaging; however, the radiation can also induce ionization processes that are potentially harmful to living systems[2]. Indeed, the targeted delivery of cytotoxic radiation to sites of disease is the cornerstone of radioimmunotherapy[3]. Chemiluminescent molecules are conceptually similar to radiotracers, but with several notable differences[4]. They are typically unstable, transient species that are generated by stoichiometric or enzymatic oxidation reactions[5]. Most chemiluminescent compounds decay by emitting visible light, which is relatively harmless and easily detected, but it is readily absorbed and scattered by the molecules and cells in biological matrices[6,7]. These factors combine to limit the utility of chemiluminescence for molecular imaging of thick tissue sections and living animals.

Here, we describe the first example of a new series of near-infrared fluorescent and chemiluminescent dyes called squaraine rotaxane endoperoxides (SREPs), and we show why they may be suitable for many types of molecular imaging and biotechnology applications. The lead structure is **1EP**, a permanently interlocked [2]rotaxane comprising a dumb-bell-shaped squaraine dye encapsulated by a tetralactam macrocycle that contains a thermally unstable 9,10-anthracene endoperoxide group (Fig. 1a)[8]. The cycloreversion reactions of aromatic endoperoxides are known to exhibit chemiluminescence, but this property has not been exploited for imaging applications[9]. As [2]rotaxanes, SREPs are well suited for programmable chemiluminescence (that is, output parameters such as emission wavelength, quantum yield and decay rate can be controlled by molecular design), because the primary source of the excitation energy (the macrocycle endoperoxide) and the emission chromophore (the encapsulated squaraine) are orthogonal molecular building blocks that are connected by a non-covalent, mechanical bond[10,11]. We report that prototype **1EP** is easily generated by simply irradiating the parent squaraine rotaxane **1** with red light in the presence of air, and that it can be stored indefinitely at −20 °C until needed. Upon warming to body temperature, **1EP** undergoes a unimolecular cycloreversion reaction that releases singlet oxygen and emits near-infrared light that can pass through a living mouse.

Results and discussion

The permanent encapsulation of squaraine **3** inside macrocycle **2** to make squaraine rotaxane **1** is achieved in high yield and large scale using straightforward synthetic methods[12]. Squaraine rotaxanes strongly absorb deep-red light and they are weak to moderate photosensitizers of molecular oxygen[13,14]. Therefore, it is not surprising that irradiation of **1** with red light in the presence of air results in a 9,10-anthracene endoperoxide product (Fig. 1b). However, the highly selective formation of mono(endoperoxide) **1EP** is noteworthy, because it contrasts with the known reactivity of the free parent macrocycle **2**, in which both anthracene units are attacked by singlet oxygen[15]. Apparently, the encapsulated squaraine prevents cycloaddition to the second anthracene unit in **1EP**. The formation of **1EP** is extremely clean (Fig. 1c); extended irradiation does not lead to any additional photochemical reaction and no chemical change occurs if air is excluded from the irradiated sample. The molecular formula and molecular connectivity of **1EP** were readily assigned by mass spectral and multidimensional nuclear magnetic resonance (NMR) methods (see Supplementary Information). Proof that the endoperoxide group is located inside the macrocycle (internal stereoisomer) was obtained using variable-temperature ^{1}H NMR spectroscopy (Supplementary Fig. S7).

Department of Chemistry and Biochemistry, 236 Nieuwland Science Hall, University of Notre Dame, Notre Dame, Indiana 46556, USA.
*e-mail: smith.115@nd.edu

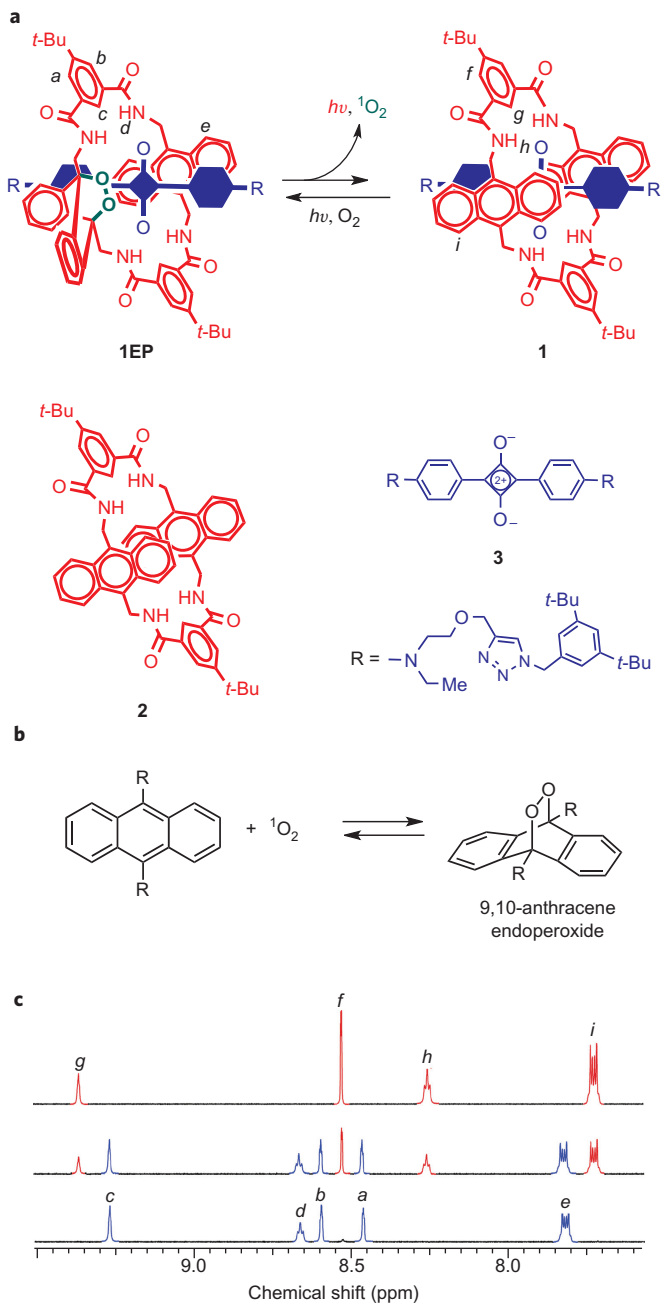

Figure 1 | Thermal cycloreversion of 1EP to 1 and reverse photoreaction. **a**, Cycloreversion of **1EP** releases singlet oxygen and emits near-infrared light. The encapsulated blue component in rotaxane **1** and **1EP** is the squaraine **3**. **b**, Formation and cycloreversion of a generic 9,10-anthracene endoperoxide. **c**, Partial ^{1}H NMR spectra ($CDCl_3$) showing photoconversion of **1** into **1EP**: (top) **1**, (middle) mixture of **1** and **1EP** after irradiation with red light for 10 min, (bottom) complete conversion to **1EP** after irradiation for 30 min.

Typically, 9,10-dialkylanthracene endoperoxides undergo skeletal rearrangements rather than cycloreversion reactions[16]. In notable contrast, endoperoxide **1EP** cycloreverts at room temperature to completely regenerate the starting squaraine rotaxane and release molecular oxygen (Supplementary Figs S9–S11). The rate constant for cycloreversion was determined by monitoring restoration of the anthracene absorption band centred at 374 nm. In *o*-xylene solvent at 38 °C, the first-order rate constant was 0.22 h^{-1}, which corresponds to a half-life of 3.2 h. Essentially the same rate constant was obtained when the solvent was changed to the more polar acetonitrile:water, 9:1. An attractive feature with SREPs is the ability to store them at low temperature for extended periods. For example, the activation energy for **1EP** cycloreversion is 113 kJ mol^{-1}, and there is no measurable reaction when samples are maintained below −20 °C. Another defining property of the endoperoxide cycloreversion process is the fraction of molecular oxygen that is released as excited-state singlet oxygen. Although the decay of singlet oxygen ($^1\Delta$) to the triplet ground state ($^3\Sigma$) can be detected directly as weak monomol ($^1O_2$) luminescence at 1,270 nm or dimol ($2\cdot{}^1O_2$) emission at 633 and 703 nm (ref. 9), it was more convenient to conduct singlet oxygen trapping experiments[17]. A number of chemical trapping agents were tested, and the most informative was 2,3-dimethyl-2-butene, which reacts with singlet oxygen to give a hydroperoxide product that is readily quantified by ^{1}H NMR spectroscopy[18]. The observed ratio of trapped hydroperoxide to regenerated squaraine rotaxane in $CDCl_3$ indicated that at least 64 ± 10% of the released molecular oxygen was singlet oxygen (Supplementary Fig. S12).

Shown in Fig. 2a is a false-colour pixel intensity map of the emission from a solution of **1EP** in $CDCl_3$ at 38 °C. The chemiluminescence decreases over time, but the decay is not a simple exponential; it is a biphasic curve with an initial rapid drop over the first few minutes followed by a slower decay with a half-life of several hours. A concentration study showed that the integrated chemiluminescence intensity for **1EP** was essentially linear over a 16-fold concentration range (Supplementary Fig. S13), indicating the potential of SREPs to act as chemiluminescent tags for quantitative detection and sensing. Furthermore, the chemiluminescence can be regenerated, as was demonstrated by experiments that irradiated an aerated sample with red light after it had decayed (Supplementary Fig. S14). Signal regeneration is not possible with radiotracers, but may be a novel way to increase chemiluminescence detection sensitivity. The image in Fig. 2a was derived from unfiltered photon counts integrated over time, but as illustrated in Fig. 2b, the emission is actually localized to the Cy5.5 filter channel (695–770 nm) of a commercial imaging station equipped with a charge-coupled device (CCD) camera. Spectral plots of the chemiluminescence and fluorescence emission for **1EP** both exhibit maxima at 733 nm (Fig. 2c), which is significantly different to the wavelength expected for dimol emission. Thus, the **1EP** chemiluminescence is emitted from the encapsulated squaraine chromophore, the excited state of which is activated during the cycloreversion process. The following experiments suggest that chromophore activation is mediated by the released singlet oxygen. First, the presence of efficient singlet oxygen quenchers, 2,3-dimethyl-2-butene or 1,4-diazabicyclo[2.2.2]octane (DABCO), in solutions of **1EP** greatly diminished the chemiluminescence intensity but had no effect on the fluorescence emission. Second, the chemiluminescence intensity for **1EP** was five times higher when the solvent was changed from $CHCl_3$ to $CDCl_3$, which correlates with longer singlet oxygen lifetime in the deuterated solvent[9]. Third, thermally generated singlet oxygen, in the absence of a chromophore, produces a weak dimol emission that is observed in the DsRed channel (575–650 nm) (Supplementary Fig. S15), but in the presence of a squaraine dye **3** there is energy transfer and dye emission in the Cy5.5 channel (Supplementary Fig. S16). An intriguing point with this latter observation is that the energy released by decay of excited-state singlet oxygen to ground-state triplet oxygen is only 94 kJ mol^{-1} and not enough to excite a squaraine chromophore to its singlet state. Previous studies of intermolecular sensitization of dye fluorescence by singlet oxygen have proposed several related mechanisms that involve dye excitation by two molecules of singlet oxygen[9,19–21]. In the specific case of **1EP** there is the additional possibility that a molecule of released singlet oxygen may excite a second molecule of **1EP** to undergo a chemiluminescent cycloreversion. Detailed mechanistic studies are ongoing, but at this point it is apparent that the chemiluminescence quantum yield for the cycloreversion of **1EP** is

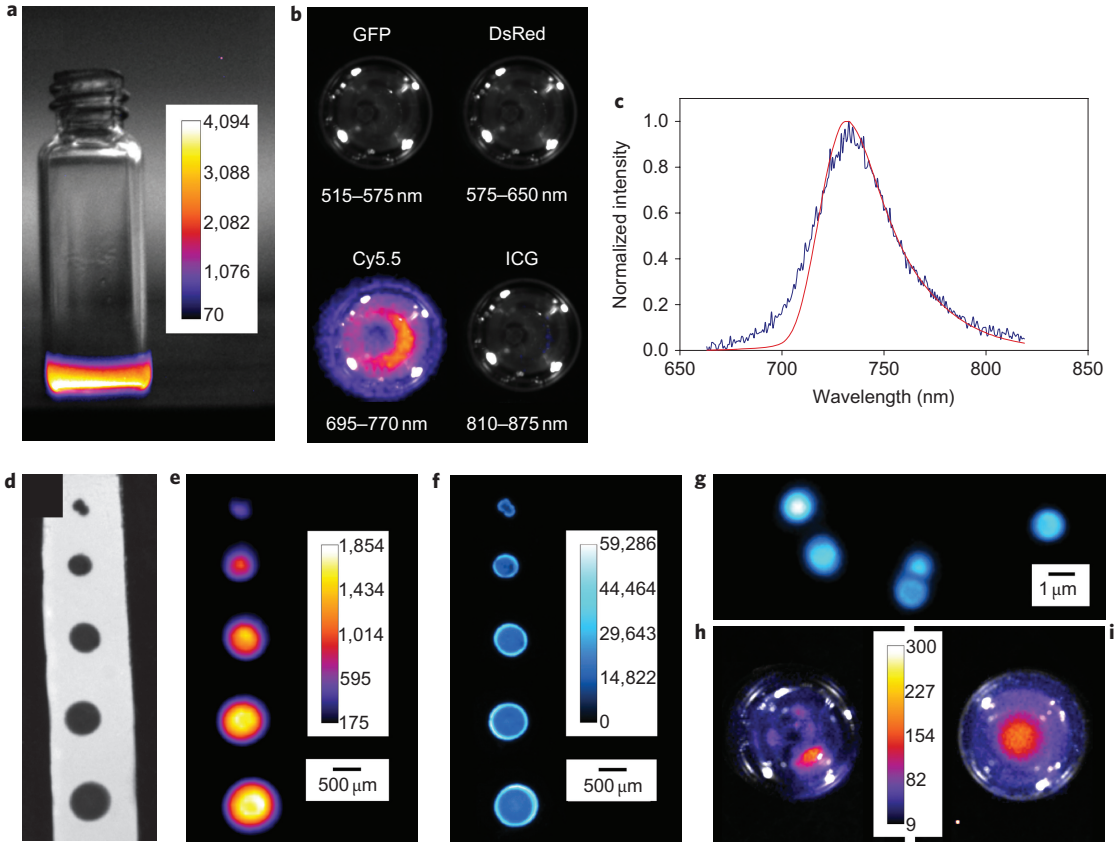

Figure 2 | False-colour pixel intensity maps at 38 °C with intensity scales in arbitrary units. a, Vial containing a solution of chemiluminescent **1EP** in $CDCl_3$. **b**, Chemiluminescence from a solution of **1EP** viewed with different emission filters. **c**, Chemiluminescence (blue) and fluorescence (red, excitation = 650 nm) emission spectra of **1EP** (1.5 mM, $C_2D_2Cl_4$) at 65 °C. **d**–**f**, Bright-field (**d**), chemiluminescence (**e**) and fluorescence (**f**) images of a reverse-phase TLC plate with spots of **1EP**. **g**, Fluorescence micrograph of carboxylate-functionalized polystyrene **1EP**-microparticles (0.9-μm diameter). **h**, Chemiluminescence from polystyrene **1EP**-microparticles that are aggregated in a vial of water (viewed from top). **i**, Chemiluminescence from carboxylate-functionalized polystyrene **1EP**-microparticles that are dispersed throughout a vial of water.

affected by the surrounding environment; it is increased by solvents and matrices that extend the singlet oxygen lifetime and raise the efficiency of intermolecular energy transfer from singlet oxygen to the encapsulated squaraine chromophore.

The potential utility in surface-based detection technologies was assessed by spotting organic solutions of **1EP** onto reverse-phase thin layer chromatography (TLC) plates (glass sheets supporting a thin layer of porous silica particles with impregnated C18 hydrocarbon). Figure 2d–f shows bright-field, chemiluminescence and fluorescence images of a surface with a progression of spot sizes. The smallest spot is ~0.2 mm in diameter, contains ~17 pmol of **1EP**, and it is easily identified using either chemiluminescence or fluorescence imaging. This highlights the detection versatility of SREPs. Both **1EP** and the decay product **1** have essentially identical near-infrared fluorescence properties, so the intrinsic bright fluorescence of a sample spot hardly changes as the chemiluminescence reaction proceeds, which means that the plate can be read by either imaging modality. In this case, the target background ratio (TBR) for fluorescence imaging is ~70, substantially better than chemiluminescence (TBR = 4.5), because background autofluorescence from the plate is very low and the squaraine chromophore is excited multiple times by the excitation beam. Commercially available, polymeric microparticles are also readily stained by treatment with **1EP** under swelling conditions (Fig. 2g)[22]. Figure 2h presents the chemiluminescence from a group of stained, polystyrene particles that are aggregated in a vial containing water, and Fig. 2i depicts an aqueous dispersion of stained polystyrene particles that have been functionalized with carboxylate groups.

For biological imaging, chemiluminescent probes have a signal contrast advantage over fluorescent probes because there is no excitation beam and thus no background autofluorescence by endogenous biomolecules[5,23,24]. However, a drawback with most of the currently available chemiluminescent and bioluminescent systems is that they emit visible light, which exhibits poor tissue penetration and large amounts of scattering[6]. The need for next-generation systems that emit light within the optimal wavelength window of 650–900 nm is well recognized[25–27]. The planar optical images in Fig. 3 illustrate the potential value of SREP-labelled microparticles or nanoparticles as chemiluminescent probes for *in vivo* imaging. An aliquot of carboxylate-functionalized **1EP**-microparticles (50 μl) was injected subcutaneously into the dorsal side of a nude mouse rear leg. Figure 3a–c shows the high-contrast chemiluminescence and reflected fluorescence dorsal images, which required light from the **1EP**-microparticles to pass through ~1 mm of skin. A region of interest (ROI) analysis indicated a TBR of 6.9 for chemiluminescence and 29 for fluorescence (Supplementary Fig. S17). Figure 3d–f presents ventral images, which required the light to penetrate a greater thickness of skin and leg tissue (~7 mm). The target signal intensities are attenuated, but the chemiluminescence TBR of 6.8 remains quite good, although the fluorescence TBR of 4.4 is considerably lower. This signal contrast advantage for chemiluminescence increases with tissue penetration distance[28], as demonstrated by the phantom experiment in Fig. 4. The top row shows that near-infrared chemiluminescence from a small tube containing a solution of **1EP** (250 nmol) passes through a living nude mouse positioned between the tube and the CCD camera. The

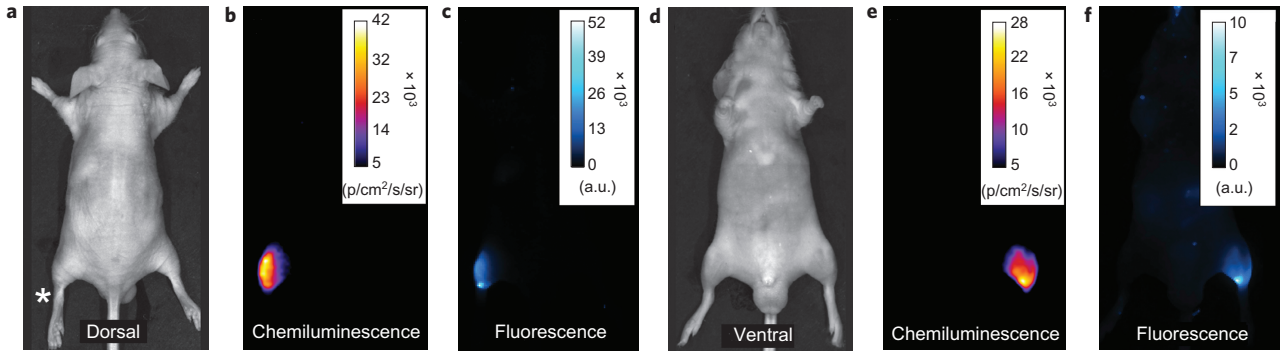

Figure 3 | Planar chemiluminescence and reflected fluorescence from 1EP-microparticles injected subcutaneously into the dorsal side of a nude mouse rear leg at 38 °C. a–c, Dorsal bright-field (**a**), chemiluminescence (**b**) and fluorescence (**c**) images (chemiluminescence and fluorescence TBR = 6.9 and 29, respectively) with injection site indicated by an asterisk. **d–f**, Ventral images, which required light penetration through deeper tissue (chemiluminescence and fluorescence TBR = 6.8 and 4.4, respectively). $N = 2$.

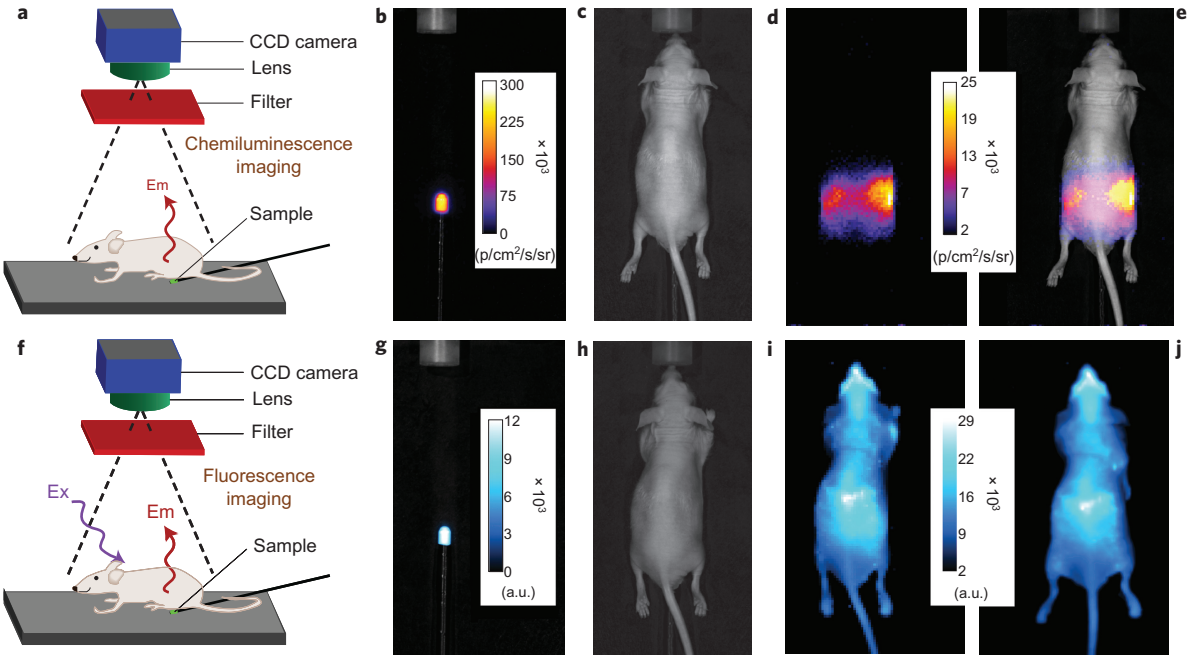

Figure 4 | Chemiluminescence from 1EP at 38 °C penetrates through a living nude mouse. a,f, Experimental set-up for planar chemiluminescence (**a**) and fluorescence (**f**) imaging, respectively. **b,g**, Chemiluminescence (**b**) and fluorescence (**g**) pixel intensities from a small tube containing **1EP** (250 nmol) in $C_2D_2Cl_4$. **c,h**, Photographs of mouse located above the tube. **d,e**, Pixel intensity map of chemiluminescence that is transmitted through the mouse (TBR = 11.6). **i**, Fluorescence intensity map of mouse located above the tube (TBR = 1.1). **j**, Fluorescence intensity map of mouse with no tube present.

TBR for the transmitted light is an impressive 11.6, although the image is quite diffuse, which is a known characteristic of planar optical imaging, even at near-infrared wavelengths[29]. Signal intensity is strongest at each side of the animal, which coincides with passage through the least amount of tissue. The bottom row in Fig. 4 depicts reflected fluorescence images of the same experimental arrangement plus excitation light; the fluorescence TBR is 1.1, and a comparison of Fig. 4i and 4j shows that fluorescence from the target site (tube containing **1EP**) cannot be readily distinguished from the background produced by scattering of the excitation light and animal autofluorescence.

Taken together, the surface and mouse imaging results indicate that chemiluminescence imaging with near-infrared **1EP** is much less 'surface-weighted' than fluorescence imaging[28]. With surface or superficial target sites, fluorescence imaging produces the best TBR, because the probe can be excited multiple times by the excitation light, which means that the target fluorescence intensity is very high. However, the TBR for planar fluorescence imaging drops quickly with tissue thickness due to an increased contribution of the background signal[24]. In comparison, the TBR for chemiluminescence imaging decreases much more gradually with tissue depth, in large part because background emission from the host animal is inherently very low. Indeed, near-infrared chemiluminescence imaging with **1EP** can produce a TBR ratio of >10 at a tissue depth of more than two centimetres. These results highlight an attractive feature of SREPs as dual-modality molecular imaging probes. They can be used in high-contrast chemiluminescence mode to locate relatively deep anatomical locations *in vivo*, and subsequently used in fluorescent mode to identify the microscopic targets within thin histopathology sections taken from the same specimen. SREPs release singlet oxygen, which is a reactive molecule and one of the primary cytotoxic agents in photodynamic therapy[30]. However, singlet oxygen is readily quenched to the triplet ground state within a cell, so the average lifetime is ~3 μs and the diffusion

radius only ~100 nm (ref. 31). Thus, the flux of singlet oxygen that is produced by stoichiometric, thermal release agents is relatively low and highly localized, which explains why they exhibit weak biological activity[32,33] and why our ongoing study of a water-soluble analogue of **1EP** has not revealed any evidence for singlet oxygen-induced cell toxicity.

Conclusions

Although many organic molecules exhibit chemiluminescence[4], there is no example of a storable compound with thermally activated near-infrared emission. SREPs, as exemplified by lead compound **1EP**, represent a new paradigm for optical molecular imaging. They are easily generated by simple irradiation of the parent squaraine rotaxane with red light in air, and they can be stored and transported at low temperature until needed. Upon warming to body temperature, SREPs emit near-infrared light that can penetrate through a living mouse with high target signal contrast. The chemiluminescent cycloreversion process hardly changes the photophysical properties of the encapsulated squaraine chromophore, so a SREP can also be detected using fluorescence, thus providing versatile dual-modality optical imaging capability. In many respects, chemiluminescent SREPs are conceptually similar to radiotracers, and they can likely be developed into the chemiluminescent equivalent of radiopharmaceuticals for complementary applications. For example, radiopharmaceuticals are suitable for deep-tissue imaging, but they emit ionizing radiation that has an inherent dosimetric health risk[34]. In contrast, chemiluminescent tracers would be restricted to shallower tissues or anatomical sites that can be reached by endoscopes. However, SREPs do not emit harmful radiation, so they may be more appropriate for longitudinal molecular imaging studies that require repeated dosing of the probe, small-animal studies that require high throughput, or imaging protocols that gain advantages by using cheaper, smaller and safer optical imaging instrumentation. We have developed robust synthetic methods for converting squaraine rotaxanes into targeted fluorescence imaging probes[8], and it should be quite feasible to incorporate SREPs within functionalized molecular constructs[35–37] or nanoparticles[38–40] to create near-infrared optical imaging agents that are both fluorescent and chemiluminescent.

Methods

Synthesis of 1EP. The known rotaxane **1**[12] (15.0 mg, 0.008 mmol) was dissolved in $CDCl_3$ (0.6 ml) and added to a standard NMR tube. The uncapped tube was placed 10 cm in front of a filtered (long-pass, 520 nm) 150 W Xenon lamp and irradiated for 30 min with exposure to atmospheric oxygen. Complete conversion to **1EP** was confirmed by ^{1}H NMR spectroscopy. The solvent was removed under reduced pressure at ice-bath temperature to give pure **1EP**, which was stored as a solid or organic solution at temperatures below −20 °C until needed. (Safety note: organic endoperoxides with high oxygen content are potentially shock-sensitive materials and should be handled in small portions.)

Staining polymeric microparticles and hydrophobic surfaces with 1EP. For the polymeric microparticles, an aliquot of tetrahydrofuran (THF, 160 μl) was added to a 2.0-ml aqueous suspension of either 1.0% (w/v) polystyrene microparticles (5.3-μm diameter, Spherotech) or carboxylate-modified polystyrene microparticles (0.9-μm diameter, Aldrich). The mixture was stirred for 1 h at room temperature, to induce particle swelling, followed by addition of a solution of **1EP** in cold THF (140 μl, 2.0 mM). After stirring for an additional 1 h at 4 °C, the mixture was centrifuged at 7,000 r.p.m. for 2 min. The blue supernatant was discarded, and the blue pellet containing the stained microparticles was washed twice by adding 1 ml of aqueous sodium dodecylsulphate (0.05% w/v) followed by centrifugation at 7,000 r.p.m. The particles were finally washed with water and resuspended in water (140 μl).

For the hydrophobic silica surface, a microsyringe was first used to make spots from a stock solution of **1EP** (1.5 mM, $CDCl_3$) on a reverse-phase TLC plate (Analtech-Uniplate) that supported a 250-μm layer of porous silica gel particles (15-μm diameter) with impregnated C18 hydrocarbon.

Chemiluminescence and fluorescence imaging. Two sets of instrumentation were used. The first made use of a Xenogen IVIS Lumina imaging system (Caliper Life Sciences) with a thermoelectrically cooled CCD camera. Solid-phase and solution samples were placed on a heated stage set to 40 °C and with a 5-cm field of view. Typically, the chemiluminescence was acquired over 60 s with 8 × 8 binning, no filter and the lens aperture fully open ($F_{stop} = 1$). Pixel intensity maps were acquired using Living Image software version 3.0, and the data were analysed using ImageJ software version 1.43r. The second set of instruments comprised an Andor iXon EMCCD camera with a thermoelectrically cooled CCD and a 25-mm lens. Solution samples were placed on a heated stage and chemiluminescent spectra were acquired using an Acton spectrometer with the monochromator set to 750 nm and a slit width of 1 mm. Fluorescence spectra were acquired with a laser (~200 μW) for excitation at 650 nm and an acquisition time of 8 ms.

Animal imaging. Animal care and handling procedures were approved by the Notre Dame Institutional Advisory Committee of Animal Care. The nude mouse (strain NCr Foxn1^{nu}) in Fig. 3 was euthanized by cervical dislocation before study, and the carcass was maintained at 38 °C using a heating pad and heated stage. The carboxylate-functionalized **1EP**-microparticles dispersed in water (50 μl, containing ~1×10^9 microparticles and 50 nmol **1EP**) were injected subcutaneously. The chemiluminescence images were acquired for 5 min with 8 × 8 binning. The fluorescence images were acquired for 1 s with 4 × 4 binning. The live nude mouse in Fig. 4 was anaesthetized using 2–3% v/v isoflurane and maintained at 1.5–2% v/v isoflurane during imaging. The tube containing **1EP** was maintained at 38 °C and the chemiluminescence images were acquired for 5 min with 8 × 8 binning. The fluorescence images were acquired for 5 s with 2 × 2 binning.

See the Supplementary Information for complete listing of spectral data, structure elucidation, kinetic analyses, control experiments and image analyses.

Received 8 July 2010; accepted 6 September 2010; published online 24 October 2010

References

1. Mettler, F. A. & Guiberteau, M. J. *Essentials of Nuclear Medicine Imaging* 5th edn (Saunders, 2005).
2. Mancini, J. G. & Ferrandino, M. N. The impact of new methods of imaging on radiation dosage delivered to patients. *Curr. Opin. Urol.* **20,** 163–168 (2010).
3. Sharkey, R. M. & Goldenberg, D. M. Novel radioimmunopharmaceuticals for cancer imaging and therapy. *Curr. Opin. Invest. Drugs* **9,** 1302–1316 (2008).
4. Roda, A., ed. *Chemiluminescence and Bioluminescence: Past, Present and Future* (Royal Society of Chemistry, 2010).
5. Su, Y., Chen, H., Wang, Z. & Lv, Y. Recent advances in chemiluminescence. *Appl. Spectrosc. Rev.* **42,** 139–176 (2007).
6. Prescher, J. A. & Contag, C. H. Guided by the light: visualizing biomolecular processes in living animals with bioluminescence. *Curr. Opin. Chem. Biol.* **14,** 80–89 (2010).
7. Roda, A., Guardigli, M., Michelini, E. & Mirasoli, M. Bioluminescence in analytical chemistry and *in vivo* imaging. *Trends Anal. Chem.* **28,** 307–322 (2009).
8. Gassensmith, J. J., Baumes, J. M. & Smith, B. D. Discovery and early development of squaraine rotaxanes. *Chem. Commun.* 6329–6338 (2009).
9. Adam, W., Kazakov, D. V. & Kazakov, V. P. Singlet-oxygen chemiluminescence in peroxide reactions. *Chem. Rev.* **105,** 3371–3387 (2005).
10. Stoddart, J. F. The chemistry of the mechanical bond. *Chem. Soc. Rev.* **38,** 1802–1820 (2009).
11. Kay, E. R., Leigh, D. A. & Zerbetto, F. Synthetic molecular motors and mechanical machines. *Angew. Chem. Int. Ed.* **46,** 72–191 (2007).
12. Gassensmith, J. J. *et al.* Synthesis and photophysical investigation of squaraine rotaxanes by 'clicked capping'. *Org. Lett.* **10,** 3343–3346 (2008).
13. Arunkumar, E., Sudeep, P. K., Kamat, P. V., Noll, B. C. & Smith, B. D. Singlet oxygen generation using iodinated squaraine and squaraine-rotaxane dyes. *New J. Chem.* **31,** 677–683 (2007).
14. Salice, P. *et al.* Photophysics of squaraine dyes: role of charge-transfer in singlet oxygen production and removal. *J. Phys. Chem. A* **114,** 2518–2525 (2010).
15. Gassensmith, J. J., Baumes, J. M., Eberhard, J. & Smith, B. D. Cycloaddition to an anthracene derived macrocyclic receptor with supramolecular control of regioselectivity. *Chem. Commun.* 2517–2519 (2009).
16. Aubry, J. M., Pierlot, C., Rigaudy, J. & Schmidt, R. Reversible binding of oxygen to aromatic compounds. *Acc. Chem. Res.* **36,** 668–675 (2003).
17. Bloodworth, A. J. & Eggelte, H. J. in *Singlet Oxygen* (ed. Frimer, A. A.) Vol. **2,** 93–203 (CRC Press, 1985).
18. Matsumoto, M., Yamada, M. & Watanabe, N. Reversible 1,4-cycloaddition of singlet oxygen to *N*-substituted 2-pyridones: 1,4-endoperoxide as a versatile chemical source of singlet oxygen. *Chem. Commun.* 483–485 (2005).
19. Fu, Y., Krasnovsky, A. A. Jr. & Foote, C. S. Singlet oxygen dimol-sensitized luminescence from thermally generated singlet oxygen. *J. Am. Chem. Soc.* **115,** 10282–10285 (1993).
20. Ishii, H., Tsukino, K., Sekine, M. & Nakata, M. Singlet oxygen-sensitized delayed emissions from hydrogen peroxide/gallic acid/potassium ferricyanide systems containing organic solvents. *Chem. Phys. Lett.* **474,** 285–289 (2009).
21. Murphy, S. T., Kondo, K. & Foote, C. S. Singlet-oxygen-sensitized delayed fluorescence: direct detection of triplet phthalocyanine as an intermediate. *J. Am. Chem. Soc.* **121,** 3751–3755 (1999).

22. Descalzo, A. B. *et al.* Phenanthrene-fused boron-dipyrromethanes as bright long-wavelength fluorophores. *Org. Lett.* **10,** 1581–1584 (2008).
23. So, M.-K., Xu, C., Loening, A. M., Gambir, S. S. & Rao, J. Self-illuminating quantum dot conjugates for *in vivo* imaging. *Nature Biotechnol.* **24,** 339–343 (2006).
24. Frangioni, J. V. The problem is background, not signal. *Mol. Imaging* **8,** 303–304 (2009).
25. Branchini, B. R. *et al.* Red-emitting luciferases for bioluminescence reporter and imaging applications. *Anal. Biochem.* **396,** 290–297 (2010).
26. le Masne de Chermont, Q. *et al.* Nanoprobes with near-infrared persistent luminescence for *in vivo* imaging. *Proc. Natl Acad. Sci. USA* **104,** 9266–9271 (2007).
27. Ma, N., Marshall, A. F. & Rao, J. Near-infrared light emitting luciferase via biomineralization. *J. Am. Chem. Soc.* **132,** 6884–6885 (2010).
28. Troy, T., Jekic-McCullen, D., Sambucetti, L. & Rice, B. Quantitative comparison of the sensitivity of detection of fluorescent and bioluminescent reporters in animal models. *Mol. Imaging* **3,** 9–23 (2004).
29. Tuchin, V. V. *Tissue Optics* 2nd edn (SPIE Press, 2007).
30. Dysart, J. S., Singh, G. & Patterson, M. S. Calculation of singlet oxygen dose from photosensitizer fluorescence and photobleaching during mTHPC photodynamic therapy of MLL cells. *Photochem. Photobiol.* **81,** 196–205 (2005).
31. Hatz, S., Poulsen, L. & Ogilby, P. R. Time-resolved singlet oxygen phosphorescence measurements from photosensitized experiments in single cells: effects of oxygen diffusion and oxygen concentration. *Photochem. Photobiol.* **81,** 1284–1290 (2008).
32. Pellieux, C., Dewilde, A., Pierlot, C. & Aubry, J.-M. Bactericidal and virucidal activities of singlet oxygen generated by thermolysis of naphthalene endoperoxides. *Method. Enzymol.* **319,** 197–207 (2000).
33. Otsu, K. *et al.* Impaired activation of caspase cascade during cell death induced by newly synthesized singlet oxygen generator, 1-buthylnaphthalene-4-propionate endoperoxide. *Cell Biol. Int.* **32,** 1380–1387 (2008).
34. Linet, M. S., Kim, K. P. & Rajaraman, P. Children's exposure to diagnostic medical radiation and cancer risk: epidemiologic and dosimetric considerations. *Pediatr. Radiol.* **39**(Supp l), S4–S26 (2009)
35. Agawa, H., Nakazono, M., Nanbu, S. & Zaitsu, K. Chemiluminescence change of polyphenol dendrimers with different core molecules. *Org. Lett.* **10,** 5171–5174 (2008).
36. Lee, C. C., Mackay, J. A., Fréchet, J. M. J. & Szoka, F. C. Designing dendrimers for biological applications. *Nature Biotechnol.* **23,** 1517–1526 (2005).
37. Xiao, S., Fu, N., Peckham, K. & Smith, B. D. Efficient synthesis of fluorescent squaraine rotaxane dendrimers. *Org. Lett.* **12,** 140–143 (2010).
38. Chatterjee, D. K., Fong, L. S. & Zhang, Y. Nanoparticles in photodynamimc therapy: an emerging paradigm. *Adv. Drug Deliver. Rev.* **60,** 1627–1637 (2008).
39. Tallury, P., Payton, K. & Swadeshmukul, S. Silica-based multimodal/multifunctional nanoparticles for bioimaging and biosensing applications. *Nanomedicine* **3,** 579–592 (2008).
40. Borisov, S. M. & Klimant, I. Luminescent nanobeads for optical sensing and imaging of dissolved oxygen. *Microchim. Acta* **164,** 7–15 (2009).

Acknowledgements

The authors are grateful to the National Science Foundation (grant no. CHE 0748761 to B.D.S.) and the University of Notre Dame Integrated Imaging Facility for financial support.

Author contributions

B.D.S. conceived this project and J.M.B. helped design the experiments. J.J.G., J.-J.L., W.J.C., A.G.W., W.M.L., J.G. and M.K. contributed to the experimental work and data analysis. B.D.S. and J.M.B. wrote the paper, and all co-authors contributed comments.

Additional information

The authors declare no competing financial interests. Supplementary information and chemical compound information accompany this paper at www.nature.com/naturechemistry. Reprints and permission information is available online at http://npg.nature.com/reprintsandpermissions/. Correspondence and requests for materials should be addressed to B.D.S.